JMEPEG (2009) 18:196–204
DOI: 10.1007/s11665-008-9283-8

1059-9495/$19.00

Corrosion of Type 7075-T73 Aluminum in a 10% HNO_3 + $Fe_2(SO_4)_3$ Deoxidizer Solution

Terence P. Savas and James C. Earthman

(Submitted April 29, 2008)

Localized corrosion damage in Type 7075-T73 aluminum was investigated for a HNO_3 + $Fe_2(SO_4)_3$ deoxidizer solution which is frequently used for surface pretreatment prior to anodizing. The corrosion damage was quantified in the time domain using the electrochemical noise resistance (*Rn*) and in the frequency domain using the spectral noise impedance (*Rsn*). The *Rsn* was derived from an equivalent electrical circuit model that represented the corrosion cell implemented in the present study. These data are correlated to scanning electron microscopy (SEM) examinations and corresponding statistical analysis based on digital image analysis of the corroded surfaces. Other data used to better understand the corrosion mechanisms include the open circuit potential (OCP) and coupling-current time records. Based on statistical analysis of the pit structures for 600 and 1200 s exposures, the best fit was achieved with a 3-paramater lognormal distribution. It was observed for the 1200 s exposure that a small population of pits continued to grow beyond a threshold critical size of 10 μm. In addition, significant grain boundary attack was observed after 1200 s exposure. These data are in good agreement with the electrochemical data. Specifically, the *Rn* was computed to be 295 and 96 Ω-cm^2 for 600 and 1200 s exposures, respectively. The calculated value of *Rsn,* theoretically shown to be equal to *Rn* in the low frequency limit, was higher than *Rn* for a 1200 s exposure period. However, better agreement between the *Rn* and *Rsn* was found for frequencies above 0.01 Hz. Experimental results on the measurement performance for potassium chloride (KCl) saturated double-junction Ag/AgCl and single-junction Hg/Hg_2Cl_2 reference electrodes in the low-pH deoxidizer solution are also compared.

Keywords 7075-T73, anodizing, deoxidizer solutions, electrochemical noise, fatigue crack initiation, scanning electron microscopy

1. Introduction

Localized pitting corrosion has been reported as a primary cause for accelerated fatigue crack nucleation in high strength aluminum alloys (Ref 1, 2). A common source for this type of corrosion is exposure to humid environments, particularly those containing acids or chlorides (Ref 3). For precipitation hardened aluminum alloys, the corrosion occurs predominantly at constituent particle locations that have lower concentrations of aluminum and thus weaker passive films (Ref 4-7). Although anodic coatings were developed to minimize corrosion during environmental exposure, the pretreatment processes used to produce these coatings can result in localized corrosion (Ref 8).

The corrosion behavior of 7075-T73 aluminum was investigated for the following categories of pretreatment solutions: (1) liquid degreasing cleaners, (2) nonetching alkaline cleaners, (3) high-pH caustic (etching) cleaners, (4) low-pH acid-based deoxidizers, and (5) low-pH sulfuric acid (for the anodize process). It was reported that the degreasing and alkaline solutions did not cause any corrosion damage while the caustic and acid-based did (Ref 8). Specifically, high-pH caustic etch solution (NaOH) was the most aggressive resulting in severe general and localized attack after exposure times in the 60-120 s range. The low-pH deoxidizer solution also caused general attack and localized pitting corrosion was observed after 600 s exposure. However, this solution was much less aggressive than the caustic etch. It was also reported that pits initiating during the pretreatment process (beyond a threshold size on the order of 10 μm) significantly increased in size during the subsequent electrochemical anodize process (sulfuric acid solution).

It was established that machined (wrought) aluminum components can be properly anodized without caustic etching if the surfaces are free of oils, greases, embedded contaminants, and oxide scale. In this case, nonetching cleaners are used in conjunction with a low-pH nitric acid-based deoxidizer. With exposure to the deoxidation solution being a required step of the anodize process, quantitative studies by means of electrochemical measurements are considered necessary to better understand the corrosion mechanisms. For most pretreatment processes the baths are agitated but there are no induced electrochemical reactions, such as in the case of the anodizing process. To properly simulate this process in a laboratory environment (i.e., localized corrosion with no system perturbations) the electrochemical noise technique was considered most appropriate (Ref 9).

Terence P. Savas, Control Systems Division, Aerospace Group, Parker Hannifin Corp, Irvine, CA 92618-1898; **Terence P. Savas**, Materials Science and Engineering Department, and **James C. Earthman**, Department of Chemical Engineering & Materials Science, University of California Irvine, Irvine, CA 92697-2575. Contact e-mails: tsavas@parker.com and earthman@uci.edu.

The measurement of current and potential fluctuations on the same electrochemical cell allows the evaluation of a quantity known as the noise resistance (*Rn*), which has been proposed as an indication of the corrosion resistance of the material under study (Ref 10-12). The measurement technique can vary somewhat, but the objective is to measure fluctuations in the current flowing between two identical coupled electrodes kept at the same potential by means of a zero-resistance ammeter (ZRA), measuring at the same time their voltage fluctuations with respect to a reference electrode (RE). The noise resistance is generally found to be inversely related to the localized corrosion rate (Ref 9) and computed over predetermined block-exposure times that vary depending on the system under study. The time-dependent electrochemical noise resistance is defined by the following:

$$Rn(t) = \frac{\sigma_V}{\sigma_I} \quad \text{(Eq 1)}$$

where σ_V and σ_I represent standard deviations of the simultaneously recorded voltage and current signals. A low value of *Rn* indicates frequent fluctuations in current transients thus signifying a high incidence of localized corrosion events. This process is a result of metastable pit nucleation and propagation, giving rise to current transients lasting on the order of 1 s, and involving a charge transfer on the order of 10^6 C (corresponding to approximately 10^{12} atoms) (Ref 13). The voltage noise scales inversely proportional to the square root of the electrode area while the current noise scales directly proportional. The *Rn* is often normalized with respect to the electrode area and is typically reported in Ω-cm^2.

Other sources of electrochemical noise have been identified. These include partial faradaic currents, adsorption/desorption processes, and hydrogen gas bubble evolution and detachment (Ref 14). For example, a hydrogen bubble can temporarily decrease the cathodic overvoltage when it rolls over the electrode surface. As a consequence, the cathodic component of the current increases and the potential is shifted in a positive direction.

The theoretical interpretation of noise is generally associated with a randomly occurring, brief pulse of charge, related to the occurrence of a single event and independent of any other event. This is known as a Poisson process, and the simplest example is the flow of electronic current in which each event is the passage of an individual electron through the measuring circuit (Ref 13).

Bertocci and coworkers reported a theoretical treatment based on modeling the corrosion cell with an equivalent electrical circuit (Ref 15). The electric circuit model simulates two identical metal electrodes, coupled in series through a ZRA and connected to an assumed noiseless RE. A saturated Ag/AgCl or Hg/Hg_2Cl_2 type RE was assumed to have negligible noise compared to the metal working electrodes. The equivalent circuit schematics for the current and voltage noise sources are illustrated in Fig. 1(a) and (b), respectively.

In the model, the noise sources, which model the random phenomena due to corrosion processes on the metal electrodes (i_1, i_2, e_1, e_2), have zero mean values. The current (I) flowing through the voltage-measuring reference electrode, immersed in the same solution, is zero due to a high input impedance (Z_{RE}). Since the electrodes are made of the same metal, the time averages of their potentials are equal and time average of the current flowing between them is zero. It should be noted that neither the individual voltage fluctuations nor the current

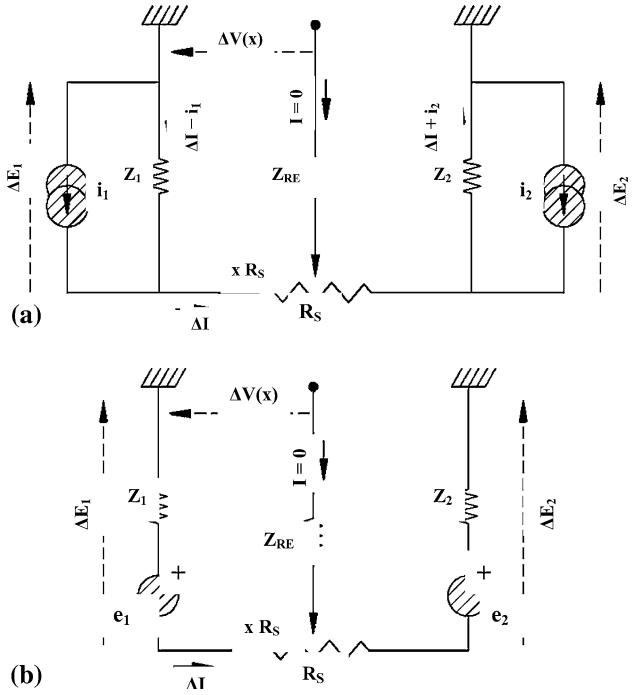

Fig. 1 Equivalent electric circuit that represents the corrosion cell used in the present study with (a) current noise sources, i_1 and i_2, and (b) voltage noise sources e_1, and e_2 (Ref 15)

fluctuations can be measured. The measurable quantities are the voltage between the coupled electrodes ($\Delta V(x)$) and RE, and the current flowing between the working electrodes (ΔI). The circuit model is simplified by the assumption that the solution resistance (*Rs*) is much lower than the impedances for the metal electrodes (*Z*1 and *Z*2). It should also be noted that the metal electrode impedance includes the double-layer capacitance. From the circuit model, Bertocci et al. derived the following relationship between the time-dependent *Rn* and the frequency-dependent spectral noise impedance, *Rsn*:

$$Rn = \left[\frac{\int_{f\,\min}^{f\,\max} \Psi_I(f) R_{sn}^2(f)\, df}{\int_{f\,\min}^{f\,\max} \Psi_I(f)\, df} \right]^{1/2} \quad \text{(Eq 2)}$$

where Ψ_I is the power spectral density (PSD) of the coupling-current, and f is the frequency, f_{min} is the lower limit frequency (equal to two times the inverse measurement time) and f_{max} is the higher limit frequency (equal to one-half the sampling frequency). The spectral noise impedance is defined as:

$$Rsn(f) = \left[\frac{\Psi_V(f)}{\Psi_I(f)} \right]^{1/2} \quad \text{(Eq 3)}$$

where Ψ_V is the PSD of the voltage signal. If f_{min} is sufficiently low (i.e., acquisition time is sufficiently long), *Rn* can be expressed by:

$$Rn = Rsn(f \to 0) \quad \text{(Eq 4)}$$

Through a theoretical analysis with a minimum number of assumptions, it was found for the case in which: (1) the

electrochemical noise (EN) sensor consisted of two identical, coupled electrodes and a noiseless RE, (2) instrumentation noise was negligible compared to the EN, and (3) the solution resistance was negligible in comparison to the electrode impedance, the following equalities existed:

$$Rn = Rsn(f \to 0) = |Z|(f = 0) = Rp \quad \text{(Eq 5)}$$

where $|Z|$ is the electrode impedance and Rp is the polarization resistance, commonly determined from linear polarization or electrochemical impedance spectroscopy (EIS) measurements. These relationships were verified experimentally for cases of bare electrodes and coated electrodes with defects (Ref 16, 17).

Mansfeld and coworkers (Ref 17) introduced a similar quantity defined as the spectral noise response:

$$R^{\circ}sn(f) = \left|\frac{V_{\mathrm{FFT}}(f)}{I_{\mathrm{FFT}}(f)}\right| \quad \text{(Eq 6)}$$

where $V_{\mathrm{FFT}}(f)$ and $I_{\mathrm{FFT}}(f)$ are the fast fourier transform of the potential and current time records simultaneously sampled. The $R^{\circ}sn$ also has the units of resistance. If only one potential and current time records are used, then the quantities defined in Eq 3 and 6 are identical since the computed values of $\psi_V(f)$ and $\psi_I(f)$ are proportional to the $|V_{\mathrm{FFT}}(f)|^2$ and $|I_{\mathrm{FFT}}(f)|^2$, respectively. Mansfeld and colleagues attempted to correlate Rn and $R^{\circ}sn$ to Rp. This was performed for several materials, solutions, and coating systems. It was reported, in general, that trends in the data were consistent although the numerical values for Rn and $R^{\circ}sn$ did not match the value of Rp determined by EIS. It was also concluded that the frequency spectra derived from the open circuit potential (OCP) were not indicative of the observed corrosion behavior. However, correlation for trends in the frequency spectra of the coupling-current time records and derived parameters Rn and $R^{\circ}sn$ were found to be in good agreement.

A wide range of information regarding theoretical and experimental aspects (including field applications) of electrochemical noise measurement can be found in the literature (Ref 11-20). However, a large majority of these studies involved chloride-containing media such as saltwater, and several were based on measurement of coating system performance. There is little information reported on solutions and corrosion processes of interest for the present study. Because of the highly aggressive nature of the nitric acid-based solution and relatively short exposure times, several challenges were expected with respect to RE performance, working electrode configuration and preparation, corrosion cell design, data acquisition, and overall experimental techniques.

The specific objectives for the present study were as follows: (1) develop a corrosion cell and experimental procedure that closely replicate an anodize pretreatment process where 7075 aluminum is exposed to a low-pH $HNO_3 + Fe_2(SO_4)_3$ (nitric acid-ferric sulfate) deoxidizer solution, (2) characterize the robustness of the corrosion measurement system using a unique setup that contains three reference electrodes, and compare the performance of double-junction Ag/AgCl and single-junction Hg/Hg_2Cl_2 reference electrodes in the deoxidizer solution, (3) perform corrosion experiments for the 7075-T73 aluminum in the deoxidizer solution and quantify the localized corrosion behavior using the time-dependent Rn and frequency-dependent Rsn parameters, and (4) perform SEM surface examinations, along with digital image analysis of the corroded surfaces, and correlate these data to the electrochemical data.

2. Procedures

2.1 Experimental Material

The as-received material consisted of Type 7075-T73 hand forged billet (Ref 19) with a 0.152 m (6 in.) square cross section and a length of 0.381 m (15 in.). To obtain the 7075 in a stabilized (overaged) T73 temper condition, the billets were solution heat treated at 744 K (880 °F) for 7 h, water quenched at room temperature, artificially aged for 6 h at 380 K (225 °F), and stabilized for 8 h at 450 K (350 °F). The stabilized temper condition reduces the strength by approximately 10% (as compared to the peak strength T6 temper) but increases the materials resistance to sensitization and subsequent stress corrosion cracking (SCC) (Ref 3). The chemical composition and mechanical properties are provided in Table 1 and 2, respectively, for the specific heat lot used in this study. Microstructural examinations (based on SEM and EDS techniques) including trends in the size, distribution, and composition of the constituent particles, for those found to induce pitting corrosion during solution exposure, can be found in (Ref 8).

2.2 Electrode and Corrosion Cell Design

The working electrodes (WEs) were extracted from the center section of the hand forged 7075-T73 billet and consisted of wafer-shaped rectangular specimens with dimensions of 6.35 cm × 3.75 cm × 0.500 cm (2.5 in. × 1.25 in. × 0.20 in.) with full radii on the edges. After final machining, the electrodes were polished down to a 600 grit finish, ultrasonically cleaned in a commercial degreasing agent, flushed with methanol, and final cleaned in a mild soap solution. It is important to note that a 'water-break-free' test was performed on the aluminum electrodes just prior to each experiment. To accomplish this, the electrode was wetted in tap water after cleaning. If there were any signs of water-breakage (beading) on the surface, it was not considered completely clean and therefore reprocessed until a 'water-break-free' surface was achieved.

Table 1 Chemical composition (wt.%) for 7073-T73 alloy evaluated in the present study

Alloy type	Cu	Fe	Si	Mn	Mg	Zn	Cr	Ti	Zr	V	Al
7075	1.5	0.26	0.07	0.020	2.4	5.6	0.19	0.02	···	···	Bal

Table 2 Mechanical properties for 7075-T73 alloy evaluated in the present study

Alloy type	Grain direction	Yield strength, MPa (ksi)	Tensile strength, MPa (ksi)	% Elongation
7075-T73	Longitudinal	381.3 (55.3)	460.5 (66.8)	15
	Long-transverse	368.9 (53.5)	449.5 (65.2)	12.5
	Short transverse	402.7 (58.4)	477.2 (69.2)	7

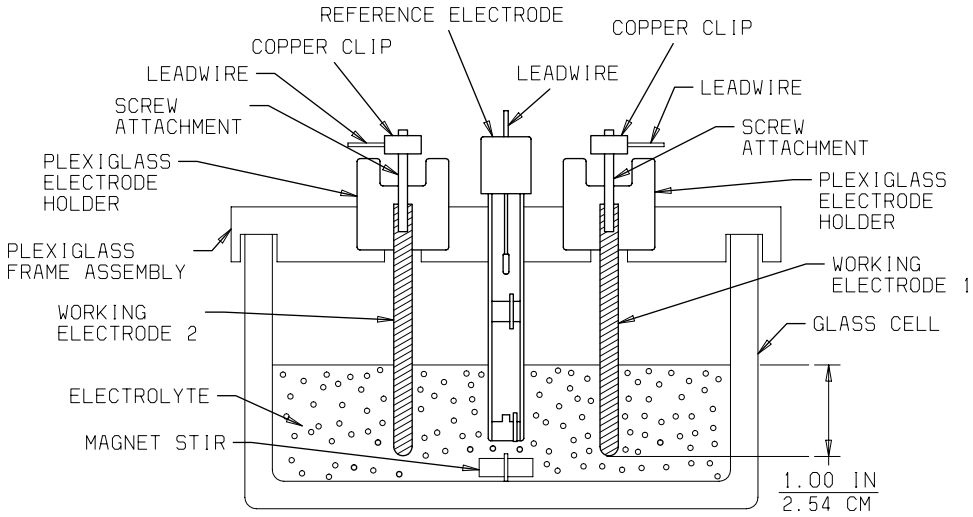

Fig. 2 Schematic of corrosion test cell for the present study

A schematic of the corrosion measurement cell developed for the present study is illustrated in Fig. 2. The cell contained 2000 mL of solution and was mounted on a magnetic stir plate. Solution agitation was used to minimize concentration gradients that could, among other factors, create a current bias between the two WEs. The solution level was maintained such that 2.54 cm (1.0 in.) of the electrode surface was submerged, resulting in 18.0 cm^2 (2.79 $in.^2$) of wetted exposure area per electrode. The two WEs were spaced 2.54 cm (1.0 in.) from the RE centerline. Note that the WEs in Fig. 2 are orientated 90º to the larger flat area of the electrodes. A stainless steel screw attachment was used to ensure a positive electrical connection and was tightened into the WEs and connected to a spring-loaded copper clip for leadwire attachment. For electrical isolation, a glass holding cell with Plexiglas electrode holder assemblies was utilized. The test cables were 100% shielded and an aluminum Faraday cage (not shown) was used to cover the cell during each experiment to prevent electromagnetic interference (EMI).

Variations between the two working electrodes can adversely influence the electrochemical noise data. Although the electrodes may appear identical, subtle differences in the as-polished surface condition, surface contamination, and solution concentration gradients can influence the measurements. These differences can result in a tendency for one electrode to polarize with respect to the other, thus leading to dc drift of the coupling-current (particularly in the early stages of exposure). For the present study, several precautions were used to effectively eliminate this problem including: (1) electrode dimensional tolerances held within ±0.0254 mm (±0.001 in.), (2) highly consistent polishing and cleaning procedures, (3) full radii on the electrode edges and corners, (4) even exposure to the acid solution by shimming the test cell (verified with a level-indicator), and (5) exposure of the WE pair to the solution at the same instant of time.

The experiments were conducted in an aqueous solution of 10% by volume of Oakite LNC™ liquid concentrate (Ref 20) at an ambient temperature of 22 °C (72 °F). This concentrate consists of approximately 20% by weight nitric acid (HNO_3) plus 60% by weight ferric sulfate ($Fe_2(SO_4)_2$) along with proprietary (inert) surfactants and wetting agents. This solution type and mixture represents the most commonly used deoxidizer for pretreatment of aluminum alloys prior to anodizing.

2.3 Electrochemical Measurements

The measurement system consisted of a three electrode cell with two identical working electrodes (WEs) connected through a zero resistance ammeter (ZRA) with a potassium chloride (KCl) saturated double-junction Ag/AgCl RE. This arrangement can be modeled by the equivalent circuit shown in Fig. 1. Some experiments were conducted with a KCl saturated single-junction Hg/Hg_2Cl_2 (calomel) RE as discussed in the following section. An ACM Instruments (Gill AC™ potentiostat) was utilized. The instrument was set in a voltage-current-time mode with the potential gain set at 10×, the over-sampling toggle turned off, and the cell settle time set to zero seconds. For the measurement sequence, a stopwatch was started, the electrodes simultaneously submerged at 10 s, with data acquisition commencing at 20 s. The majority of corrosion experiments were conducted for 1200 s whereas the RE measurements were conducted for 600 s. The data sampling rate ranged between 10 and 50 Hz. However, the majority of the data were acquired at 10 Hz. The characteristics of the noise for this particular material and solution were such that 10 Hz proved to be an adequate sampling rate. This was verified by experiment where the differences were found negligible by use of either frequency extreme. The lower sampling rate was desirable for data file management.

It was of interest to validate the corrosion measurement system by using only reference electrodes (REs). The setup was as previously described except that the two metal WEs were replaced with identical REs, resulting in a three RE cell configuration. The reason for this test was twofold: first to make certain the noise associated with the measurement system was orders of magnitude lower than that for the aluminum specimens, and second, to characterize and compare the performance of the Ag/AgCl and Hg/Hg_2Cl_2 REs in a low-pH (≤ 1) acid solution.

The measured solution resistance (*Rs*) in the present study was 1.4 Ω, a small fraction of the electrode impedance and considered negligible with respect to data interpretation. If the *Rs* is not negligible with respect to the electrode impedance, the

value of the voltage can vary depending on the positioning of the electrodes within the solution (Ref 16). In the present study, experiments were conducted to study the effect of electrode spacing. These data were not affected by the placement confirming the hypothesis that the solution resistance was negligible for the present system under study.

2.4 Quantitative Analysis

Digital image analysis was used to quantify the pit sizes and distributions along with metallographic cross-sectioning. Image analysis was conducted for samples exposed to the deoxidation solution for 600 and 1200 s exposures. This technique requires converting gray-scale SEM micrographs of the corroded surfaces into black and white binary images, and then digitizing the image. The image analysis software (Image-Pro™, Media Cybernetics) then provides various size and distribution parameters associated with the binary image features. These data were analyzed with statistical analyses to quantify the corrosion damage and correlated to the electrochemical data. With this technique, the pit diameters and pit areas are commonly computed.

3. Results

3.1 Reference Electrode Measurements

Voltage and coupling-current time records are presented in Fig. 3(a) and (b), respectively, for the KCl saturated double-junction Ag/AgCl and single-junction Hg/Hg_2Cl_2 REs.

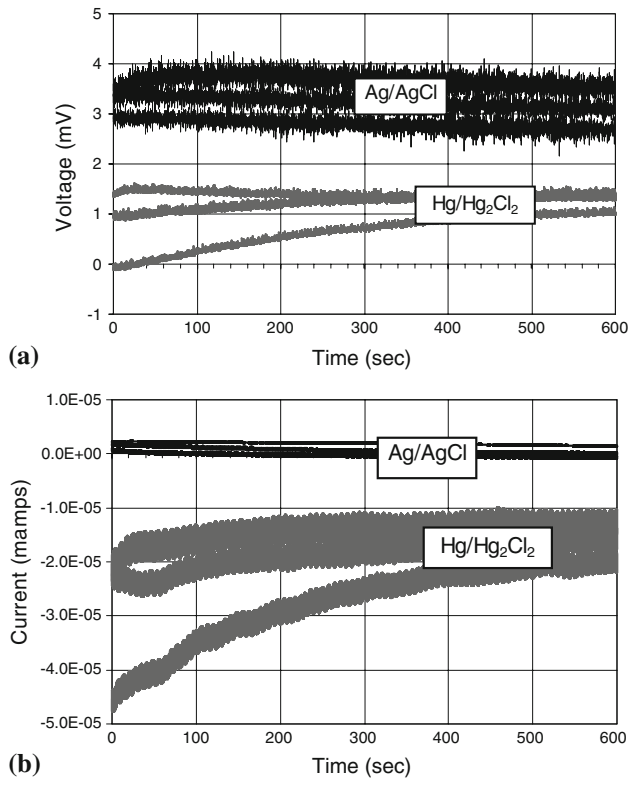

Fig. 3 Voltage (a) and coupling-current (b) time records representing three experiments each for the potassium chloride (KCl) saturated double-junction Ag/AgCl and single-junction Hg/Hg_2Cl_2 reference electrodes in a 10% HNO_3 + $Fe_2(SO_4)_3$ aqueous solution

These data represent three separate experiments. Trends in data indicate the Ag/AgCl exhibited higher peak-to-peak voltage noise amplitude, on the order of 0.50 mV, compared to the Hg/Hg_2Cl_2 amplitude of 0.20 mV. The Hg/Hg_2Cl_2 did exhibit a higher tendency for voltage drift; however, after stabilization, the stability of the voltage was comparable to the Ag/AgCl. The coupling-current traces showed the opposite behavior where the noise amplitude of the Hg/Hg_2Cl_2 was an order of magnitude higher than the Ag/AgCl, in the range of 5 nanoamps. The dc drift was again more pronounced with the Hg/Hg_2Cl_2. Figures 4(a) and (b) illustrate the same data provided in Fig. 3, however, rescaled on the time axis to better reveal the characteristics of the noise. The noise resistance versus time for the two electrode types, derived from the voltage and current data in Fig. 3, is illustrated in Fig. 5. The average *Rn* for the 600 s exposure period was approximately 5×10^5 Ω and 3.5×10^4 Ω for the Ag/AgCl and Hg/Hg_2Cl_2, respectively. Thus, the Ag/AgCl showed a significantly higher noise resistance than the Hg/Hg_2Cl_2 in the low-pH deoxidizer solution. Since the numerical value of *Rn* is directly proportional to the voltage noise and inversely proportional to the current noise, these data were in good agreement.

Power spectral density (PSD) plots, derived from the voltage and current data shown in Fig. 3, are illustrated in Fig. 6. It was difficult to draw any conclusions from the voltage PSD since the spectra appeared similar for both types of electrodes. However, the current PSD for the Hg/Hg_2Cl_2 was a factor of one hundred higher than that for Ag/AgCl. Since the current PSD is indicative of the system power output as a function of

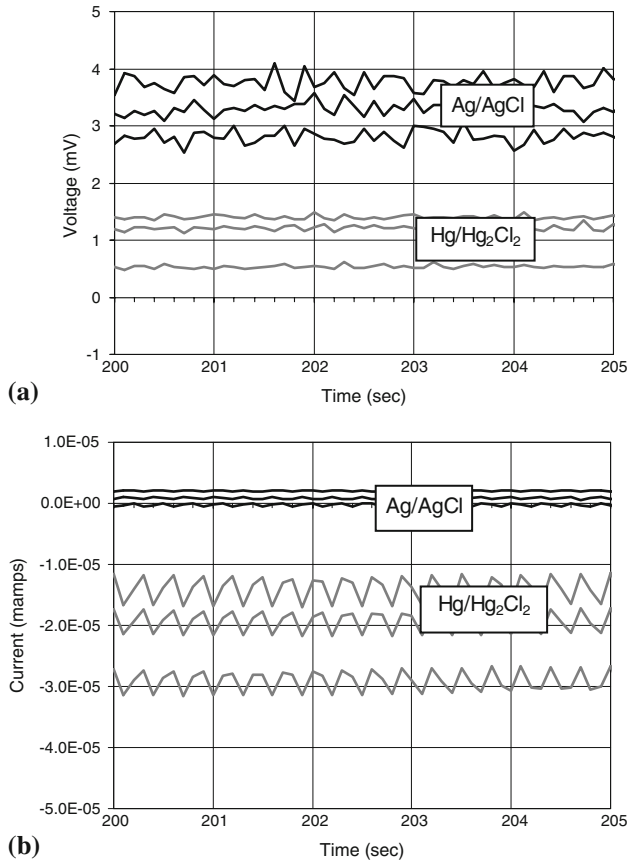

Fig. 4 Data from Fig. 3 rescaled on the time axis to better reveal the characteristic voltage (a) and current noise (b)

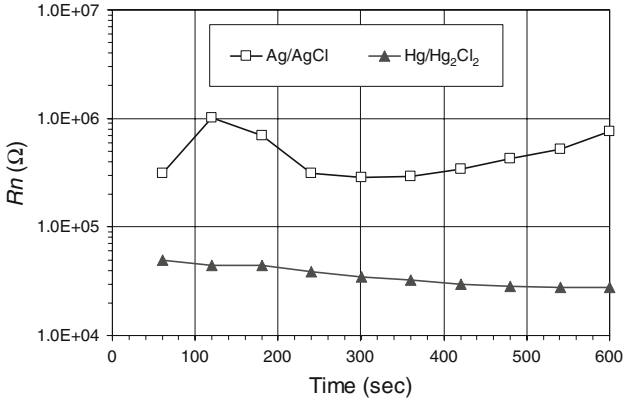

Fig. 5 Electrochemical noise resistance (*Rn*) derived from the voltage and current time records provided in Fig. 3

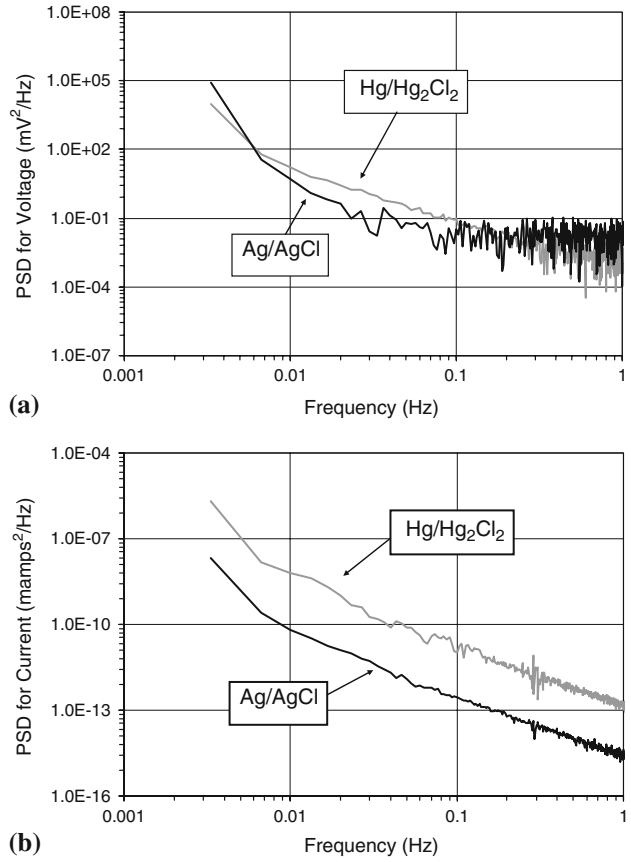

Fig. 6 PSD for voltage (a) and coupling-current (b) noise signals for the double-junction Ag/AgCl and single-junction Hg/Hg_2Cl_2 reference electrodes in a 10% HNO_3 + $Fe_2(SO_4)_3$ aqueous solution

frequency, and an order of magnitude higher current noise was observed for the Hg/Hg_2Cl_2 (Fig. 3b), these data were also in good agreement. Figure 7 shows the corresponding spectral noise impedance (*Rsn*) derived from the voltage and current PSDs provided in Fig. 6. In this case, the value at the low frequency limit (0.0033 Hz) was computed to be 1.94×10^6 Ω for the Ag/AgCl and 6.63×10^4 Ω for Hg/Hg_2Cl_2. In comparison to the *Rn* values, the *Rsn* was an approximate factor of four higher for the Ag/AgCl and factor of two higher for the Hg/Hg_2Cl_2. It can be observed that although *Rsn* is numerically

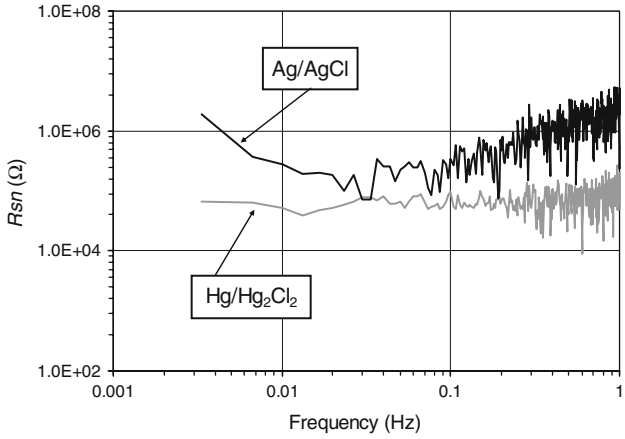

Fig. 7 Spectral noise resistance (*Rsn*) derived from the voltage and current PSDs provided in Fig. 6

greater than *Rn*, trends in these data are consistent. For the Ag/AgCl, the value of the *Rsn* was closer in numerical value to the *Rn* at frequencies above 0.01 Hz.

Searson and Dawson (Ref 21) performed a similar study comparing the noise characteristics of Ag/AgCl and Hg/Hg_2Cl_2 REs immersed in aerated sea water. It was reported that Hg/Hg_2Cl_2 exhibited rapid changes in potential but of relatively low amplitude (typically less than 10 μV) whereas the Ag/AgCl showed slower changes in potential but the magnitude was often several millivolts. The Ag/AgCl type exhibited a higher amplitude noise spectra of −35 dB/$(Hz)^{1/2}$ while the Hg/Hg_2Cl_2 RE had a noise level of −78 dB/$(Hz)^{1/2}$ in the low frequency limit. These data are consistent with findings in the present study in that the Hg/Hg_2Cl_2 showed lower voltage noise amplitude. However, the overall noise resistance and impedance were found to be higher for the Ag/AgCl type.

3.2 Corrosion Measurements

Figure 8 shows the OCP and coupling-current time records for 7075-T73 alloy in the deoxidizer solution. The OCP initiated at approximately −130 mV with a steep gradient to a more steady-state value of −40 mV after 400 s. Unlike a theoretically perfect system, the coupling-current exhibited an initial polarization of one electrode on the order of 0.05 to 0.1 mamps/cm^2. After approximately 400 s (in conjunction with the voltage signal) the electrodes reached a steady-state condition for the remainder of the exposure. However, a small bias current on the order of 25-50 μamp/cm^2 was present throughout the entire exposure. This was attributed to slight differences between the WEs with respect to factors previously described. Figure 9 shows the corresponding *Rn* derived from the voltage and current data in Fig. 8. The results for the aluminum are normalized with respect to the electrode area (previously reported as 18.0 cm^2 for each WE). After 600 s, a time commonly used in practice, the *Rn* was computed to be 295 Ω-cm^2. The *Rn* after 1200 s exposure was 96 Ω-cm^2. This duration represented an over-exposure due, for example, to poor process controls. These values are based on the average data for three separate experiments.

The observed corrosion behavior, based on the overall shape of the *Rn*-time trace, exhibited a fairly steep drop after 240 s and then begins to climb at 480 s. This was attributed to re-passivation effects for a certain number of metastable pits.

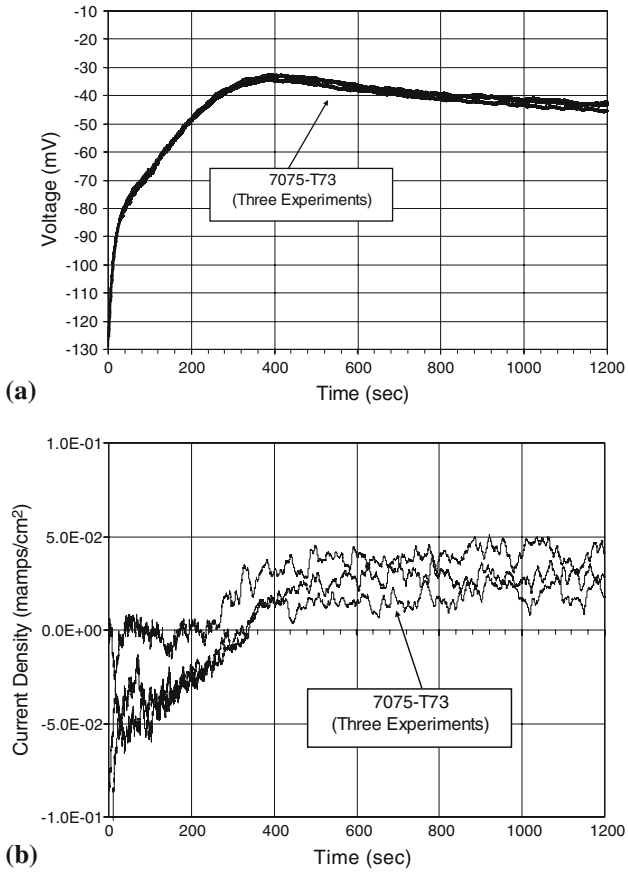

Fig. 8 Simultaneously recorded OCP (a) and coupling-current (b) versus time for 7075-T73 electrodes in a 10% HNO_3 + $Fe_2(SO_4)_3$ aqueous solution (RE: Ag/AgCl)

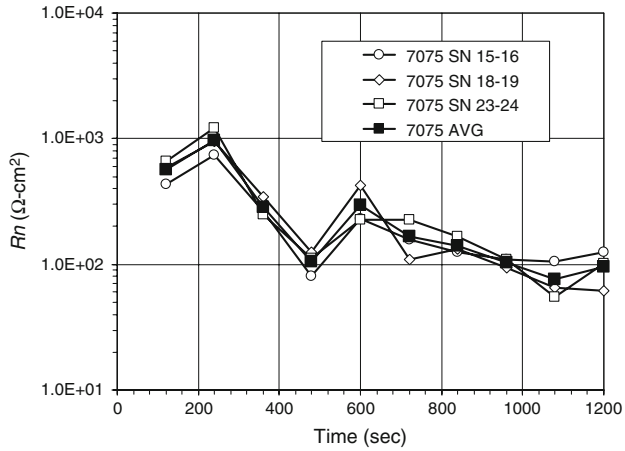

Fig. 9 Electrochemical noise resistance (*Rn*) for 7075-T73 alloy derived from the voltage and current time records provided in Fig. 8 (RE: Ag/AgCl)

The drift downward at 600 s and the significantly lower *Rn* for 1200 s exposure were attributed to the continued growth of a small population of pits and the onset of grain boundary attack that appeared as numerous micropits at high magnification.

The *Rsn* for the 7075-T73 alloy derived from a 1200 s time record is provided in Fig. 10. In this case, the *Rsn* in the low frequency limit was computed to be 4.45×10^3 Ω-cm^2 for

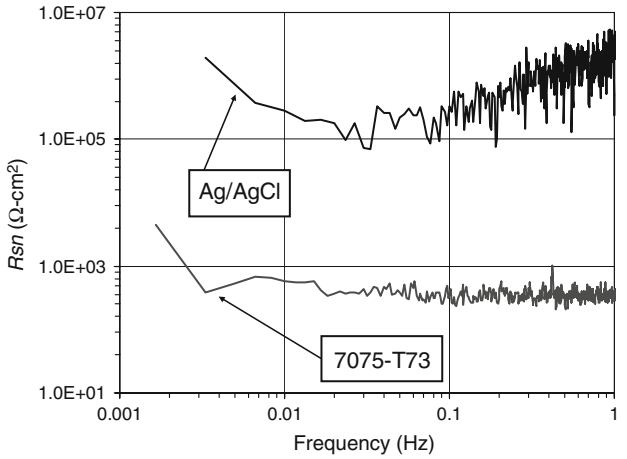

Fig. 10 *Rsn(f)* versus frequency for aluminum 7075-T73 and Ag/AgCl working electrodes RE in a 10% HNO_3 + $Fe_2(SO_4)_3$ aqueous solution. Note: the PSDs were determined for 600 s and 1200 s exposures for the 7075-T73 and Ag/AgCl, respectively

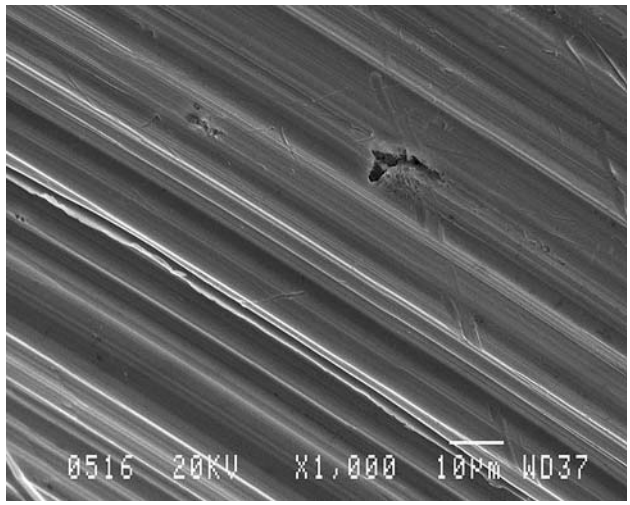

Fig. 11 As-polished surface of 7075-T73 electrode. A typical micropit is evident that was presumably introduced initiated during the pre-exposure cleaning or polishing process (1000×)

7075-T73. Similar to the trends in the RE only results, the numerical value of the *Rsn* in the low frequency limit (in this case, 0.00167 Hz) was found to be higher than *Rn*. However, at frequencies above 0.01 Hz, the numerical values were much closer, on the order of 300-400 Ω-cm^2. The *Rsn* for the Ag/AgCl RE is also provided for reference to show the measurement system has orders of magnitude higher impedance than the aluminum samples under study, thus confirming the robustness of the setup with respect to characterizing their corrosion behavior.

3.3 Surface Examinations

Figure 11 is a micrograph of an as-polished 7075-T73 electrode surface with a single isolated micropit present, presumably initiated during the pre-exposure cleaning or polishing process. Figure 12 shows typical corrosion damage after 600 and 1200 s exposures to the deoxidizer solution, respectively. Based on visual examination of the micrographs,

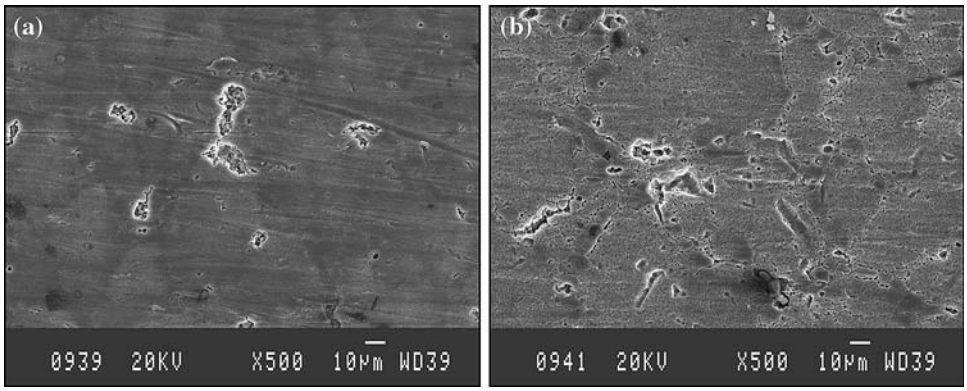

Fig. 12 7075-T73 surface appearance after 600 s (a) and 1200 s (b) exposure to 10% HNO_3 + $Fe_2(SO_4)_3$ aqueous solution (500×)

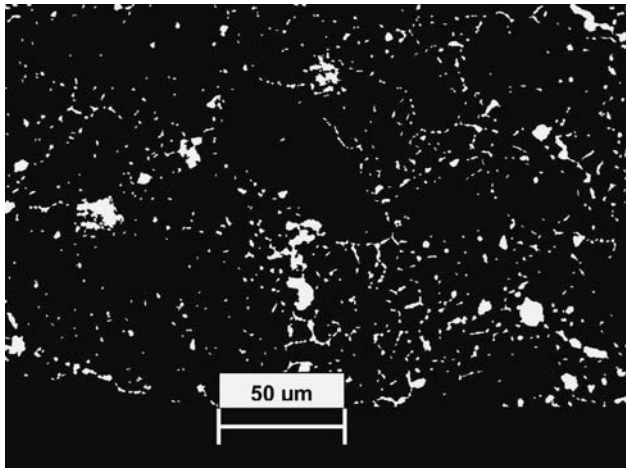

Fig. 13 Image analysis results for 7075-T73 after 1200 s exposure to a 10% HNO_3 + $Fe_2(SO_4)_3$ aqueous solution (500×)

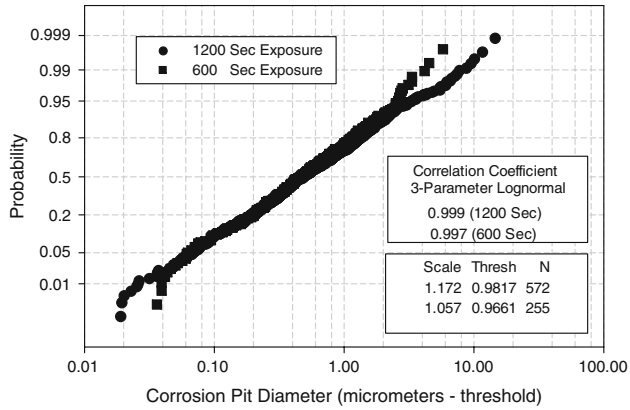

Fig. 14 Probability plot for 3-paramater lognormal distribution of corrosion pit diameters for 7075-T73 exposed to 10% HNO_3 + $Fe_2(SO_4)_3$ aqueous solution for 600 and 1200 s durations

it was apparent the 600 s exposure resulted in (mild) general attack of the surface, for example, smoothening of the polishing grooves (apparent in Fig. 11) and regions of localized pitting corrosion. The 1200 s exposure resulted in a more severe general attack (or roughening of the surface), slightly larger and more frequent pit structures, and significant grain boundary attack. The dimensions of the various defects can be estimated from the micrographs.

It can also be observed in Fig. 12(b) that the pitting mechanisms included selective dissolution where the particles are anodic with respect to the matrix phase, and circumferential attack, where the particles are noble. For the present study, the latter mechanism was much more predominant. It was previously reported (Ref 8) that particles high in Fe and Cu concentration were prone to selective dissolution, while particles high in Mg and Si concentration were prone to circumferential attack for this specific material and solution.

To accurately quantify the corrosion damage, digital image analysis techniques were utilized. As previously described, SEM micrographs of the corroded surfaces were converted into binary images to quantify the various corrosion pits. Figure 13 shows a typical image analysis micrograph for a 1200 s exposure. Probability plots that were generated using the image analysis data for 600 and 1200 s exposures are illustrated in Fig. 14. The best fit straight line was achieved with a 3-paramater lognormal distribution. For this type of distribution a scale factor must be added to *x*-axis value to obtain the actual pit size (Ref 22). The following can be observed from these data: (1) the average pit diameter was approximately 1 µm for the 600 and 1200 s exposures, (2) the largest pit diameter was approximately 10 µm (for 600 s exposure) and 15 µm for 1200 s exposure, (3) the 1200 exposure created a significantly higher population of pits beyond a threshold critical size of 10 µm in diameter, and (4) a higher population of smaller pits was observed for the 1200 s exposure, attributed to grain boundary attack. Based on metallographic cross sections (not shown) the maximum and average pit depths were measured to be 9.1 and 4.1 µm, respectively, for a 600 s exposure.

4. Summary and Conclusions

The present study focused on electrochemical corrosion behavior of Type 7075-T73 aluminum exposed to a low-pH HNO_3 + $Fe_2(SO_4)_3$ (nitric acid-ferric sulfate) deoxidizer solution. This solution is commonly used for the pretreatment of aluminum prior to anodizing. The localized corrosion that can occur during solution exposure is a primary concern for accelerated fatigue crack nucleation for fracture-critical components. The corrosion damage was characterized in the time domain using the electrochemical noise resistance (*Rn*) and in the frequency domain using the spectral noise impedance (*Rsn*).

The electrochemical data were then correlated to surface examinations that consisted of SEM and statistical analysis based on digital image analysis of the corroded surfaces.

Close correlation was found between the time-dependent *Rn* determined from electrochemical measurements and the severity of localized corrosion damage as revealed by SEM surface examinations, and corresponding digital image analysis of the corroded surfaces. Specifically, for a 600 s exposure the *Rn* was computed to be 295 Ω-cm^2 corresponding to a maximum (typical) pit diameter of 10 μm. For a 1200 s exposure, the *Rn* was computed to be 96 Ω-cm^2 corresponding to a maximum pit diameter of 15 μm (Fig. 9 and 14). The pitting corrosion was found to be particle-induced and both selective dissolution and circumferential attack mechanisms were identified. In addition, significant intergranular attack was apparent after 1200 s exposure. The intergranular attack, when viewed at high magnification, also appeared to be particle-induced and consisted of a high population of micropits (Fig. 12b).

The present results emphasize the importance of proper process controls for fracture-critical high strength aluminum components since these defects can greatly accelerate fatigue crack nucleation (Ref 1, 2). In addition, if the pretreatment process results in pit structures beyond a threshold size (on the order of 10 μm) it was reported they can significantly grow in size and depth during a subsequent anodizing process (Ref 8). Further studies should be aimed at reduced exposure times, for example, in the 200-400 s range, and how shorter durations influence the integrity of the anodic coating.

The present experiments have confirmed with reasonable accuracy that spectral noise impedance (*Rsn*) is proportional to the working electrode impedance if a noiseless reference electrode is used. Based on the present analysis, the time-dependent noise resistance (*Rn*) is approximately equal to the frequency-dependent spectral noise impedance (*Rsn*) in the low frequency limit if certain conditions are satisfied. In the present investigation, it was found that the value of the *Rsn* was higher than *Rn* in the low frequency limit. However, a closer correlation was observed at frequencies above 0.010 Hz. In addition, the internal noise generated by otherwise identical electrodes is not an obstacle to useful results, nor is the existence of a nonzero average current between the current-measuring electrodes.

It has been observed that metal electrodes prepared and treated in exactly the same way can exhibit significantly different electrochemical behavior. It was found in the present study that several measures can be implemented to minimize this behavior. However, these successful results should not be overshadowed by the fact that these types of measurements can pose several challenges.

Acknowledgment

The financial support of Parker Aerospace, Irvine, California, is gratefully acknowledged.

References

1. E.J. Dolley, B. Lee, and R.P. Wei, The Effect of Pitting Corrosion on Fatigue Life, *Fatigue Fracture Eng. Mater. Struct.*, 2000, **23**, p 555–560
2. P.S. Pao, S.J. Gill, and C.R. Feng, On Fatigue Crack Initiation from Corrosion Pits in 7075–T7351 Aluminum Alloy, *Scripta Mater.*, 1998, **43**(5), p 391–396
3. ASM International, *Metals Handbook*, 9th ed., Vol 13, Corrosion, Materials Park, Ohio, 1987, p 550–552
4. R.P. Wei, C. Liao, and G. Gao, A Transmission Electron Microscopy Study of Constituent-Particle-Induced Corrosion in 7075-T6 and 2024-T3 Aluminum Alloys, *Metall. Mater. Trans. A*, 1998, **29A**, p 1153–1160, April
5. E.E. Stansbury and R.A. Buchanan, *Fundamentals of Electrochemical Corrosion*, ASM International, 2002
6. G.S. Frankel, Pitting Corrosion of Metals—A Summary of Critical Factors, *J. Appl. Electrochem.*, 1998, **145**, p 2186
7. G.S. Frankel, *Localized Corrosion of Metals; Review of the Rate-Controlling Factors in Initiation and Growth*, Passivity-8, Jasper, Canada, Keynote Address, May 1999
8. T.P. Savas and J.C. Earthman, Surface Characterization of 7075-T73 Aluminum Exposed to Anodizing Pretreatment Solutions, *J. Test. Eval.*, JTEVA, On-Line, ISSN: 1544-1024, March 2008
9. J.R. Kearns, J.R. Scully, P.R. Roberge, D.L. Reichart, J.L. Dawson, *Electrochemical Noise Measurements for Corrosion Applications*, ASTM STP 1277, American Society for Testing and Materials, 1996
10. R.A. Cottis, M.A.A. Al-Awadhi, H. Al-Mazeedi, and S. Turgoose, Measures for the Detection of Localized Corrosion with Electrochemical Noise, *Electrochim. Acta*, 2001, **46**(24–25), p 3665–3674
11. R.A. Cottis, M.A. Al-Ansari, G. Bagley, and A. Pettiti, Electrochemical Noise Measurements for Corrosion Studies, *Mater. Sci. Forums*, 1998, **289–292**, p 741–754
12. T.P. Savas, J.C. Earthman, and A.Y.-L. Wang, The Effect of Heat Treatment on the Corrosion Resistance of 440C Stainless in 20% HNO_3 + 2.5% $Na_2CR_2O_7$ Solution, *JMEP*, April 2003
13. R.A. Cottis, The Interpretation of Electrochemical Noise Data, *Corrosion*, 2001, **27**(3), p 265–285
14. X.Y. Zhou, et al., Quantitative Evaluation of General Corrosion of Type 304 Stainless Steel in Sub-Critical and Supercritical Aqueous Solutions Via Electrochemical Noise Analysis, *Corros. Sci.*, 2002, **44**, p 841–860
15. U. Bertocci, C. Gabrielli, F. Huet, and M. Keddam, Noise Resistance Applied to Corrosion Measurements, I. Theoretical Analysis, *J. Electrochem. Soc.*, 1997, **144**(1), p 31–37, January
16. U. Bertocci, C. Gabrielli, F. Huet, M. Keddam, and P. Rousseau, Noise Resistance Applied to Corrosion Measurements, II. Experimental Tests, *J. Electrochem. Soc.*, 1998, **145**(8), p 2780–2786
17. F. Mansfeld, H. Xiao, and Y. Wang, Evaluation of Localized Corrosion Phenomena with Electrochemical Impedance Spectroscopy (EIS) and Electrochemical Noise Analysis (ENA), *Mater. Sci. Forums*, 1995, **192–194**, p 673–692
18. F. Mansfeld and H. Xiao, Electrochemical Noise Analysis of Iron Exposed to NaCl Solutions of Different Corrosivity, *J. Electrochem. Soc.*, 1993, **140**(8), p 2205–2209
19. Anon.: AMS-A–22771, Aluminum Alloy Forgings, Heat Treated, SAE International, June 1999
20. Oakite LNC Liquid Non-Chromated Deoxidizer Product Data Sheet, Chemetall Oakite Corporation, New Providence, NJ 07974, USA, 1992
21. P.C. Searson and J.L. Dawson, Analysis of Electrochemical Noise Generated by Corroding Electrodes Under Open-Circuit Conditions, *J. Electrochem. Soc.*, 1988, **135**(8), p 1908–1915
22. P. Hoang, *Springer Handbook of Engineering Statistics*, Springer-Verlag Publishing, London, 2006